Anti-tubercular activity of novel 4-anilinoquinolines and 4-anilinoquinazolines

Christopher R. M. Asquith[a,b], Neil Fleck[c], Chad D. Torrice[d], Daniel J. Crona[d,e], Christoph Grundner[c,f,*], William J. Zuercher[b,e,*]

[a]*Department of Pharmacology, School of Medicine, University of North Carolina at Chapel Hill, Chapel Hill, NC 27599, USA*
[b]*Structural Genomics Consortium, UNC Eshelman School of Pharmacy, University of North Carolina at Chapel Hill, Chapel Hill, NC 27599, USA*
[c]*Seattle Children's Research Institute, Seattle, WA 98101, USA*
[d] *Division of Pharmacotherapy and Experimental Therapeutics, UNC Eshelman School of Pharmacy, University of North Carolina at Chapel Hill, Chapel Hill, NC 27599, USA.*
[e] *Lineberger Comprehensive Cancer Center, University of North Carolina at Chapel Hill, Chapel Hill, NC 27599, USA*
[f] *Department of Global Health, University of Washington, Seattle, WA 98195, USA.*

ARTICLE INFO

Article history:
Received
Revised
Accepted
Available online

Keywords:
Anti-tubercular
4-anilinoquinoline
4-anilinoquinazoline
Mycobacterium tuberculosis (*Mtb*)

ABSTRACT

We screened a series of 4-anilinoquinolines and 4-anilinoquinazolines and identified novel inhibitors of *Mycobacterium tuberculosis* (*Mtb*). The focused 4-anilinoquinoline/quinazoline scaffold arrays yielded compounds with high potency and the identification of 6,7-dimethoxy-*N*-(4-((4-methylbenzyl)oxy)phenyl)quinolin-4-amine (**34**) with an MIC_{90} value of 0.63-1.25 µM. We also defined a series of key structural features, including the benzyloxy aniline and the 6,7-dimethoxy quinoline ring, that are important for *Mtb* inhibition. Importantly the compounds showed very limited toxicity and scope for further improvement by iterative medicinal chemistry.

Mycobacterium tuberculosis (*Mtb*), the causative agent of tuberculosis (TB) in humans,[1] infects nearly a third of the earth's population and caused 1.6 million worldwide deaths in 2017.[2] With nearly ten million new cases of active disease each year, TB is now the leading cause of death from infectious disease globally.[2] Current therapeutic strategies involve the use of a combination of anti-microbial agents including ethambutol, isoniazid, pyrazinamide and rifampicin (Fig. 1).[3] However, more than 5% of *Mtb* infections now involve multidrug-resistant (MDR-TB) and

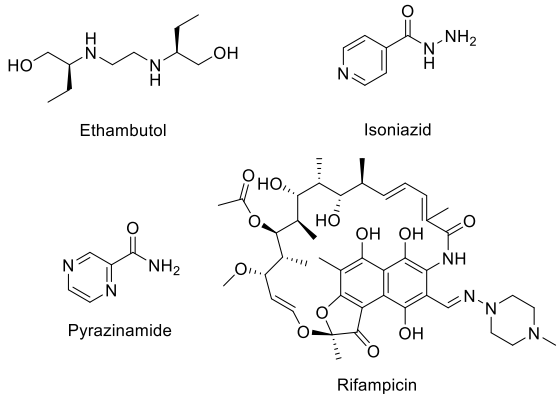

Figure 1. Current therapeutic strategies for treatment of *Mycobacterium tuberculosis* infections.

∗ Corresponding authors: e-mail: Christoph.Grundner@seattlechildrens.org (C. Grundner), william.zuercher@unc.edu (W. J. Zuercher)

extensively drug-resistant (XDR-TB) *Mtb* strains. MDR-TB is associated with a 50% mortality rate whereas XDR-TB is nearly always fatal.[4] There is an urgent need for new therapeutic strategies.

Human protein kinases are pharmacologically tractable enzymes targeted by more than three dozen approved medicines.[5] Hundreds of additional kinase inhibitors are under clinical and preclinical investigation. There is growing recognition that pathogen kinases may be targeted in the treatment of infectious diseases.[6-7] Considering the conserved ATP-binding site across species, we looked to screen collections of ATP-competitive inhibitors of human kinases for their anti-tubercular activity.

To identify new chemical starting points against *Mtb* we looked to lapatinib, gefitinib, and erlotinib as starting points which have recently been revealed to have activity against *Mtb* (Fig. 2.).[5,8] We tested the activity of lapatinib, gefitinib, and erlotinib against *Mtb* by measuring luminescence and growth on solid medium across a series of four two-fold dilutions starting at 20 µM (Tab 1).[9-10] The reduction of visible growth on solid medium demonstrated the compounds to be bactericidal.

Gefitinib treatment had no effect relative to the absence of compound. Erlotinib induced a modest effect that appeared to

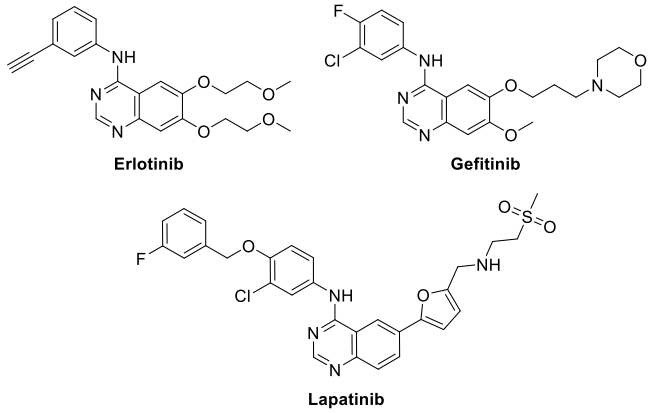

Figure 2. Structures of clinical quinazolines.

Table 1. Results of clinical inhibitors.

Compound	*Mtb* signal[a]					WS-1[b]
/μM	1.25	2.5	5	10	20	(μM)
Gefitinib	1.08	1.09	1.05	1.08	1.05	23
Erlotinib	1.05	0.96	0.9	0.68	0.7	8.6
Lapatinib	0.99	0.9	0.74	0.17	0.08	13

[a]Relative luminescence measured at 3 days after treatment. Values = RLU(sample)/RLU(no compound) at μM concentrations and no effect at 0.625 μM; [b]ref[11]

plateau at a signal of approximately 70 %. In contrast, lapatinib showed activity even at 5 μM and reduced the relative *Mtb* signal to below 10 % at 20 μM. This result suggested that the 4-benzyloxy aniline substituent might be important for anti-*Mtb* activity. These compounds demonstrate only limited toxicity in a human skin fibroblast cell line (WS-1) counter screen.[11]

To further explore quinazoline *Mtb* activity, we profiled several focused arrays of compounds to probe the structure activity relationships of the quinoline/quinazoline. We hence synthesized a series of compounds (**1**-**34**) following up on the results listed in table 1, exploring the 4-anilinoquinoline and 4-anilinoquinazoline scaffolds through nucleophilic aromatic displacement of 4-chloroquin(az)olines. (Sch. 1) We were able to access products in good to excellent yields (55-91 %) consistent with previous reports and without protection of the alcohol substituted quin(az)oline starting material.[11-13]

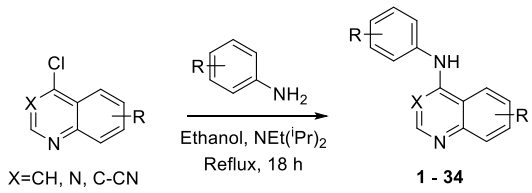

Scheme 1. General synthetic procedure

The first set of compounds probed a replacement of the 6-postion morpholine segment of gefitinib with a simple alcohol on the lapatinib scaffold (Tab. 2).[20] Although neither the 6-OH (**1**) or 7-OH (**2**) quinazoline showed appreciable activity, the 6,7-dihydroxy compound (**3**) began to inhibit *Mtb* growth at higher concentrations. The analogous set of methoxy-substituted compounds (**4**-**6**) had very similar activity profiles. The 6-OH quinoline (**7**) showed improved activity relative to the matched quinazoline (**1**). The inclusion of fluorine substitution on the phenyl ring distal to the quinazoline (**8**-**10**) led to markedly increased activity for all three isomers. At 20 μM, **8**-**10** all reduced

Table 2. Results of alcohol replacement of lapatinib and gefitinib (**1**-**12**).

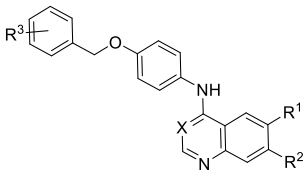

Compound	X	R^1	R^2	R^3	*Mtb* signal[a] (μM)					WS-1[b]
					1.25	2.5	5	10	20	(μM)
1	N	OH	H	H	0.95	0.94	0.96	0.90	0.80	26
2	N	H	OH	H	0.90	0.90	0.89	0.88	0.89	>100
3	N	OH	OH	H	0.95	0.93	0.91	0.76	0.69	8.8
4	N	OMe	H	H	1.04	1.07	0.89	0.83	0.62	>100
5	N	H	OMe	H	1.05	1.12	0.99	0.87	0.64	>100
6	N	OMe	OMe	H	1.04	1.04	0.83	0.77	0.6	>100
7	CH	OH	H	H	0.95	0.86	0.66	0.42	0.37	2.5
8	N	OH	H	4-F	0.86	0.76	0.64	0.44	0.32	>100
9	N	OH	H	3-F	0.76	0.64	0.49	0.39	0.25	12
10	N	OH	H	2-F	0.89	0.82	0.63	0.46	0.28	28
11	N	H	OH	4-F	0.94	1.01	0.90	0.89	0.83	>100
12	N	OH	OH	4-F	1.04	1.14	1.00	0.89	0.76	>100

[a]Relative luminescence measured at 3 days after treatment. Values = RLU(sample)/RLU(no compound) at μM concentrations and no effect at 0.625 μM; [b]IC_{50} (mean average n=4), 48 h

Table 3. Matched pair comparison of structures similar to erlotinib and lapatinib (**13**-**28**).

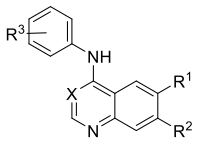

Compound	R^1	R^2	X	R^3	*Mtb* signal[a,b]			WS-1[c]
					5 μM	10 μM	20 μM	(μM)
13	CF_3	H	CH	3,4,5-$(OMe)_3$	1.23	1.14	1.21	>100
14	CF_3	H	N	3,4,5-$(OMe)_3$	1.25	1.12	1.06	>100
15	Br	H	CH	3,4,5-$(OMe)_3$	1.35	1.41	1.28	>100

16	OMe	OMe	CH	3,4,5-$(OMe)_3$	1.26	1.11	1.06	>100
17	OMe	OMe	N	3,4,5-$(OMe)_3$	1.03	1.01	0.94	>100
18	OMe	OMe	CN	3,4,5-$(OMe)_3$	1.03	1.01	0.97	>100
19	6,7-$(OCH_2CH_2OMe)_2$		N	3,4,5-$(OMe)_3$	1.02	0.96	0.87	>100
20	6,7-$(OCH_2CH_2OMe)_2$		CH	3-Ethynyl	0.88	0.79	0.58	>100
21	OMe	OMe	CH	3-Ethynyl	1.02	0.89	0.67	>100
22	OMe	OMe	N	3-Ethynyl	0.93	0.83	0.69	>100
23	OMe	OMe	CN	3-Ethynyl	1.08	1.03	0.98	>100
24	OMe	OMe	CH	3-Bromo	1.03	0.90	0.6	9.6
25	OMe	OMe	N	3-Bromo	0.98	0.71	0.65	3.9
26	OMe	OMe	CN	3-Bromo	0.88	0.56	0.37	11
27	OMe	OMe	N	3-Cl-4-(2-F-PhO)	0.92	0.74	0.80	1.1
28	OMe	OMe	CH	3-Cl-4-(2-F-PhO)	0.78	0.22	0.10	11

[a]Relative luminescence was measured at 3 days after treatment. Values = RLU(sample)/RLU(no compound); [b]None of the compounds reduced the relative *Mtb* signal below 95 % at 1.3 or 2.5 μM; [c]IC_{50} (mean average n = 4), 48 h

the relative *Mtb* signal to 25-37 %, and a modest but discernable reduction in signal was observed at 1.25 μM. Interestingly, the effect of fluorine substitution led to a different activity pattern from changing quinazoline ring substitution as the modification of **1** to the 7-OH (**11**) or 6,7-$(OH)_2$ (**12**) resulted in a significant loss of activity, even at 20 μM. These results demonstrated that *Mtb* activity was sensitive to changes at multiple parts of the template and that these changes were not necessarily additive. We counter screened **1**-**12** in human skin fibroblast cells (WS-1) and observed very limited toxicity with **3** and **7** the only compounds in the single digit micromolar range (IC_{50} = 8.8 and 2.5 μM respectively).[15]

The next set of quin(az)olines profiled was prepared to explore the contributions from both the aniline and the core heterocycle (Tab. 3).[11,16] The larger 3,4,5-trimethoxyphenyl aniline was employed on several diversely substituted quinolines and quinazolines (**13**-**18**) which led to no observable activity except when paired with the 6,7-$(OCH_2CH_2OMe)_2$-quinazoline of erlotinib (**19**) which had only slight activity at 20 μM. On the other hand, incorporation of the aniline fragment from erlotinib (3-ethynylphenyl) did yield several active compounds, including the quinoline analog of erlotinib (**20**). The erlotinib aniline with a 6,7-$(OMe)_2$-substituted quinoline core (**21**) or quinazoline (**22**) showed activity but not with the 3-cyanoquinoline (**23**). The analogous 3-bromophenyl aniline compounds (**24**-**26**) showed higher activity than the paired 3-ethynylphenyl compounds. Finally, the aniline substitution from lapatinib (3-Cl-4-(2-F-PhO)Ph) yielded a marginally active quinazoline (**27**) and a highly active quinoline (**28**) that had 10 % *Mtb* signal at 20 μM. We counter screened **13**-**28** in WS-1 cells and observed limited toxicity in most compounds. However, the bromine substitution appeared to increase toxicity (**24**-**26**) along with the lapatinib derivatives (**27**-**28**).

A subsequent set of compounds explored features of the 4-benzyloxyaniline portion of the quinoline template (Tab. 4).[17-18] Variation of the ether linkage to an amide and addition of a hydroxy on the aniline portion revealed an activity pattern where 6,7-dimethoxy substitution with the benzylic arm was active (**29**-**30**). In contrast, truncation of the benzyl also removed the activity as in acetamide **31,** which had no effect on *Mtb*. The 6-methoxy (**32**) and 7-methoxy (**33**) showed no reduction in *Mtb* signal at 20 μM. However, switching back to the 4-methyl benzyl ether linked compound **34** yielded the most potent activity observed with any compound in the present study, with a robust signal observed even at 1.25 μM. The *Mtb* MIC_{90} for **34** was in the 0.63-1.25 μM range. However, the kill curve plateaued at 5 μM, and no improved killing was observed at higher doses (98 % inhibition at 5 μM; 98 % inhibition at 20 μM) (Fig. 3).

As with the other compound sets, we evaluated **29**-**34** in human skin fibroblast cells (WS-1) and observed moderate toxicity in the single digit micromolar range for most compounds.[20] Importantly, the anti-*Mtb* effects of compounds appeared to be divergent from the toxic effects in WS-1 cells, suggesting that the *Mtb* effects were not driven by nonspecific cytotoxicity. The most potent anti-*Mtb* compound **34** had WS-1 IC_{50} = 5.4 μM, substantially higher than its *Mtb* MIC_{90} value and within threefold of the IC_{50} values for erlotinib and lapatinib. This result demonstrated that, in the human WS-1 cell line, **34** behaved comparably to two approved medicines.

These structure activity relationships between *Mtb* activity and the 4-anilinoquinoline/quinazoline scaffold have the potential to inform a medicinal chemistry strategy for enhanced *Mtb* activity. The most sensitive structural changes were found to be in the ring appended to the aniline rather than in the quin(az)oline core.

This body of work provides a number of exciting starting points for further optimization, with limited non-specific toxicity. However, the failure to achieve complete parasite kill led us to deprioritize the series due to the potential for resistance to develop. The mechanism of anti-*Mtb* activity of the quin(az)olines has yet to be defined. These compounds were originally prepared as inhibitors of human kinases targeting the ATP-binding site, a

Table 4. Matched pair comparison of benzyloxyaniline.

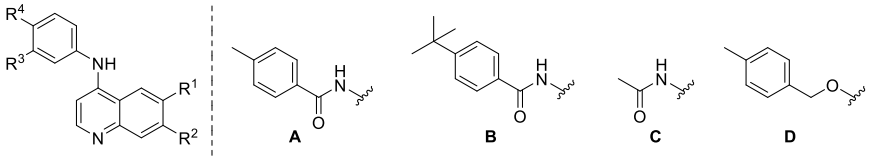

Compound	R^1	R^2	R^3	R^4	*Mtb* signal[a] (μM)					WS-1[b]
					1.25	2.5	5	10	20	(μM)
29	OMe	OMe	OH	**A**	1.14	1.09	1.13	1.05	0.45	16

30	OMe	OMe	OH	**B**	1.10	1.12	1.06	0.72	0.25	2.6
31	OMe	OMe	H	**C**	1.21	1.10	1.11	1.07	1.02	9.7
32	OMe	H	OH	**A**	1.11	1.17	1.14	1.28	0.95	10
33	H	OMe	OH	**A**	1.13	1.11	1.09	1.11	0.96	4.7
34	OMe	OMe	H	**D**	0.43	0.17	0.10	0.08	0.09	5.4

[a]Relative luminescence was measured at 3 days after treatment. Values = RLU(sample)/RLU(no compound); [b]IC_{50} (mean average n=4), 48 h

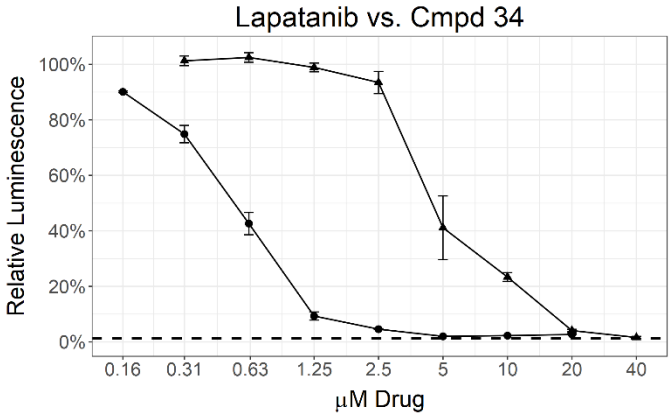

Figure 3. MIC determination by two different assays for **34** (circle) and lapatanib (triangle). Data points represent the mean of 3 biological replicates with standard deviation. The dashed line labeled 1% inoculum represents an inoculation of 1 % of the number of cells used for compound testing. This control was used to determine 99 % inhibition of growth.

rational starting hypothesis for the mechanism of action is that the effects of these compounds are mediated by inhibition of *Mtb* kinases. However, it is possible that the observed phenotypes may originate from modulation of other, non-kinase ATP-binding proteins in the organism.

Gefitinib, erlotinib, and lapatinib have previously been reported to inhibit the intracellular growth of *Mtb*. Multiple lines of evidence were described suggesting inhibition of the host target epidermal growth factor receptor (EGFR) was responsible for this activity.[15] However our results demonstrate that proteins within the pathogen itself may be targeted as well. The benzyl substituent present in the molecule showed a pivotal effect to potency, as is highlighted by the enhanced activity of **34** relative to **30**. The present results help define a de-risked medicinal chemistry trajectory towards anti-tubercular compounds with targets in both the host and the parasite itself. Such dual acting compounds might offer advantages in efficacy and/or reduction in propensity for resistance.

Acknowledgments

The SGC is a registered charity (number 1097737) that receives funds from AbbVie, Bayer Pharma AG, Boehringer Ingelheim, Canada Foundation for Innovation, Eshelman Institute for Innovation, Genome Canada, Innovative Medi-cines Initiative (EU/EFPIA) [ULTRA-DD grant no. 115766], Janssen, Merck KGaA Darmstadt Germany, MSD, Novartis Pharma AG, Ontario Ministry of Economic Development and Innovation, Pfizer, São Paulo Research Foundation-FAPESP, Takeda, and Wellcome [106169/ZZ14/Z]. C. G. is supported by R01 AI117023 from the NIH/NIAID**.** We are grateful Dr. Brandie Ehrmann for LC-MS/HRMS support provided by the Mass Spectrometry Core Laboratory at the University of North Carolina at Chapel Hill.

References and notes

1. Pai, M.; Behr, M. A.; Dowdy, D.; Dheda, K.; Divangahi, M.; Boehme, C. C.; Ginsberg, A.; Swaminathan, S.; Spigelman, M.; Getahun, H.; Menzies, D.; Raviglione, M. *Nat Rev Dis Primers* **2016**, *2*, 16076.
2. World Health Organization. Global Tuberculosis Report 2018 (WHO, **2018**).
3. Chan, E. D.; Iseman, M. D. *BMJ.* **2002**, *325*, 1282.
4. Floyd, K.; Glaziou, P.; Zumla, A.; Raviglione, M. *Lancet Respir Med* **2018**, *6*, 299.
5. Ferguson, F. M.; Gray, N. S. *Nat Rev Drug Discov.* **2018**, *17*, 353.
6. Sachan, M.; Srivastava, A.; Ranjan. R.; Gupta, A.; Pandya, S.; Misra, A. *Curr Pharm Des.* **2016**, *22*, 2599.
7. Glennon, E. K. K.; Dankwa, S.; Smith, J. D.; Kaushansky, A. *Trends Parasitol.* **2018**, *34*, 843.
8. Stanley, S. A.; Barczak, A. K.; Silvis, M. R.; Luo, S. S.; Sogi, K.; Vokes, M.; Bray, M. A.; Carpenter, A. E.; Moore, C. B.; Siddiqi, N.; Rubin, E. J.; Hung, D. T. *PLoS Pathog.* **2014**, *10*, e1003946.
9. Andreu, N.; Fletcher, T.; Krishnan, N.; Wiles, S.; Robertson, B. D. *J Antimicrob Chemother.* **2012**, *67*, 404.
10. An H37Rv strain containing an auto-luminescence operon (LuxABCDE) was grown to log phase, diluted and re-grown for at least 2 doublings to a final OD_{600} of 0.005. Cultures were dispensed into 96-well white, flat-bottom plates in 100 µL final volume. Luminescence was quantified using a PHERTAstar plate reader (BMG Labtech) blanked against 7H9 media.
11. Asquith, C. R. M.; Naegeli, K. M.; East, M. P.; Laitinen, T.; Havener, T. M.; Wells, C. I.; Johnson, G. L.; Drewry, D. H.; Zuercher, W. J.; Morris, D. C. *J Med Chem.* **2019**, 62, 4772.
12. Asquith, C. R. M.; Laitinen, T.; Bennett, J. M.; Godoi, P. H.; East, M. P.; Tizzard, G. J.; Graves, L. M.; Johnson, G. L.; Dornsife, R. E.; Wells, C. I.; Elkins, J. M.; Willson, T. M.; Zuercher, W. J. *ChemMedChem* **2018**, *13*, 48.
13. Asquith, C. R. M.; Treiber, D. K.; Zuercher, W. J. *Bioorg Med Chem Lett.* **2019**, *29*, 1727.
14. **General procedure for the synthesis of 4-anilinoquin(az)olines**: 4-chloroquin(az)oline derivative (1.0 eq.), aniline derivative (1.1 eq.), and $^{i}Pr_2NEt$ (2.5 eq.) were suspended in ethanol (10 mL) and refluxed for 18 h. The crude mixture was purified by flash chromatography using EtOAc:hexane followed by 1-5 % methanol in EtOAc; After solvent removal under reduced pressure, the product was obtained as a free following solid or recrystallized from ethanol/water.

4-{[4-(benzyloxy)phenyl]amino}quinazolin-6-ol (**1**) as a yellow solid (68 %, 220 mg, 0.640 mmol) MP 231-233 °C; ^{1}H NMR (400 MHz, DMSO-d_6) δ 11.21 (s, 1H), 10.91 (s, 1H), 8.75 (s, 1H), 8.04 (d, J = 2.5 Hz, 1H), 7.88 (d, J = 9.0 Hz, 1H), 7.70 (dd, J = 9.1, 2.5 Hz, 1H), 7.62 – 7.57 (m, 2H), 7.52 – 7.44 (m, 2H), 7.44 – 7.37 (m, 2H), 7.37 – 7.30 (m, 1H), 7.14 – 7.09 (m, 2H), 5.16 (s, 2H). ^{13}C NMR (101 MHz, DMSO-d_6) δ 158.8, 157.8, 156.7, 148.1, 136.9, 131.6, 129.7, 128.5 (2C, s), 127.9, 127.7 (2C, s), 126.5, 126.2 (2C, s), 121.2, 114.92, 114.85 (2C, s), 107.1, 69.4. HRMS m/z $[M+H]^+$ calcd for $C_{21}H_{18}N_3O_2$: 344.1399 found = 344.1386; LC t_R = 4.24 min, >98% Purity.

4-{[4-(benzyloxy)phenyl]amino}quinazolin-7-ol (**2**) as a light yellow solid (78 %, 223 mg, 0.648 mmol) MP 277-279 °C; ^{1}H NMR (400 MHz, DMSO-d_6) δ 11.76 (s, 1H), 11.42 (s, 1H), 8.76 (d, J = 9.0 Hz, 1H), 8.74 (s, 1H), 7.59 – 7.54 (m, 2H), 7.49 – 7.44 (m, 2H), 7.42 – 7.38 (m, 2H), 7.36 – 7.28 (m, 3H), 7.12 – 7.07 (m, 2H), 5.15 (s, 2H). ^{13}C NMR (101 MHz, DMSO-d_6) δ 164.3, 158.9, 156.6, 150.5, 140.4, 136.9, 129.7, 128.5 (2C, s), 127.9, 127.7 (2C, s), 127.1, 126.3 (2C, s), 119.4, 114.8 (2C, s), 105.8, 102.0, 69.4. HRMS m/z $[M+H]^+$ calcd for $C_{21}H_{18}N_3O_2$: 344.1399 found = 344.1386; LC t_R = 4.33 min, >98% Purity.

4-{[4-(benzyloxy)phenyl]amino}quinazoline-6,7-diol (**3**) as a light yellow solid (69 %, 189 mg, 0.527 mmol) MP 272-274 °C; ^{1}H NMR (400 MHz, DMSO-d_6) δ 10.32 (s, 2H), 8.53 (s, 1H), 7.91 (s, 1H), 7.64 – 7.53 (m, 2H), 7.50 – 7.44 (m, 2H), 7.43 – 7.37 (m, 2H), 7.36 – 7.30 (m, 2H), 7.20 (s, 1H), 7.10 – 7.01 (m, 2H), 5.13 (s, 2H). ^{13}C NMR (101 MHz, DMSO-d_6) δ 157.4, 155.7, 154.3, 149.1, 147.7, 137.1, 131.2, 128.5 (2C, s), 127.8, 127.7 (2C, s), 125.4 (2C, s), 114.7 (2C, s), 107.3, 106.7, 104.9, 69.4. HRMS m/z $[M+H]^+$

calcd for $C_{21}H_{18}N_3O_3$: 360.1348 found = 360.1335; LC t_R = 4.22 min, >98% Purity.

***N*-(4-(benzyloxy)phenyl)-6-methoxyquinazolin-4-amine** (**4**) as a light yellow solid (84 %, 231 mg, 0.647 mmol) MP 270-272 °C; ^{1}H NMR (400 MHz, DMSO-d_6) δ 11.64 (s, 1H), 8.79 (s, 1H), 8.41 (d, *J* = 2.6 Hz, 1H), 7.92 (d, *J* = 9.1 Hz, 1H), 7.72 (dd, *J* = 9.2, 2.5 Hz, 1H), 7.68 – 7.53 (m, 2H), 7.53 – 7.18 (m, 5H), 7.18 – 7.04 (m, 2H), 5.17 (s, 2H), 4.00 (s, 3H). ^{13}C NMR (101 MHz, DMSO-d_6) δ 159.0 (2C, s), 156.8, 148.8, 136.9, 133.3, 129.6, 128.5 (2C, s), 127.9, 127.7 (2C, s), 126.8, 126.4 (2C, s), 121.4, 114.9 (2C, s), 114.6, 104.6, 69.4, 56.7. HRMS m/z $[M+H]^+$ calcd for $C_{22}H_{19}N_3O_2$: 357.1477 found = 358.1546; LC t_R = 4.53 min, >98% Purity.

***N*-[4-(benzyloxy)phenyl]-7-methoxyquinazolin-4-amine** (**5**) as a colourless solid (91 %, 251 mg, 0.701 mmol) MP 247-249 °C; ^{1}H NMR (400 MHz, DMSO-d_6) δ 11.58 (s, 1H), 8.87 (d, *J* = 9.3 Hz, 1H), 8.81 (s, 1H), 7.71 – 7.57 (m, 2H), 7.58 – 7.12 (m, 7H), 7.13 – 6.99 (m, 2H), 5.15 (s, 2H), 3.97 (s, 3H). ^{13}C NMR (101 MHz, DMSO-d_6) δ 164.7, 158.9, 156.7, 150.8, 140.7, 136.9, 129.6, 128.5 (2C, s), 127.9, 127.7 (2C, s), 127.0, 126.3 (2C, s), 118.7, 114.8 (2C, s), 107.1, 100.1, 69.4, 56.3. HRMS m/z $[M+H]^+$ calcd for $C_{22}H_{19}N_3O_2$: 357.1477 found = 358.1547; LC t_R = 4.49 min, >98% Purity.

***N*-(4-(benzyloxy)phenyl)-6,7-dimethoxyquinazolin-4-amine** (**6**) as a colourless solid (84 %, 217 mg, 0.561 mmol) MP 250-252 °C; ^{1}H NMR (400 MHz, DMSO-d_6) δ 11.44 (s, 1H), 8.73 (s, 1H), 8.36 (s, 1H), 7.68 – 7.56 (m, 2H), 7.55 – 7.43 (m, 2H), 7.43 – 7.15 (m, 4H), 7.15 – 7.03 (m, 2H), 5.15 (s, 2H), 4.00 (s, 3H), 3.96 (s, 3H). ^{13}C NMR (101 MHz, DMSO-d_6) δ 157.9, 156.5, 156.0, 150.0, 148.6, 137.0, 135.5, 129.9, 128.5 (2C, s), 127.9, 127.7 (2C, s), 126.3 (2C, s), 114.8 (2C, s), 107.1, 104.1, 99.8, 69.4, 57.0, 56.4. HRMS m/z $[M+H]^+$ calcd for $C_{23}H_{21}N_3O_3$: 388.1661 found = 388.1651; LC t_R = 4.55 min, >98% Purity.

4-{[4-(benzyloxy)phenyl]amino}quinolin-6-ol (**7**) as a light yellow solid (64 %, 182 mg, 0.532 mmol) MP 218-220 °C; ^{1}H NMR (400 MHz, DMSO-d_6) δ 10.67 (s, 1H), 10.37 (s, 1H), 8.32 (d, *J* = 6.8 Hz, 1H), 7.96 (d, *J* = 9.1 Hz, 1H), 7.91 (d, *J* = 2.5 Hz, 1H), 7.63 (dd, *J* = 9.1, 2.4 Hz, 1H), 7.58 – 7.44 (m, 2H), 7.46 – 7.22 (m, 5H), 7.23 – 7.13 (m, 2H), 6.57 (d, *J* = 6.8 Hz, 1H), 5.17 (s, 2H). ^{13}C NMR (101 MHz, DMSO-d_6) δ 157.3, 156.5, 154.1, 140.1, 136.8, 132.2, 130.2, 128.5 (2C, s), 128.0, 127.8 (2C, s), 127.2 (2C, s), 124.9, 121.9, 118.7, 116.0 (2C, s), 105.4, 98.6, 69.5. HRMS m/z $[M+H]^+$ calcd for $C_{22}H_{19}N_2O_2$: 343.1447 found = 343.1433; LC t_R = 4.45 min, >98% Purity.

4-({4-[(4-fluorophenyl)methoxy]phenyl}amino)quinazolin-6-ol (**8**) as a yellow solid (76 %, 228 mg, 0.631 mmol) Decomposed >200 °C; ^{1}H NMR (400 MHz, DMSO-d_6) δ 11.22 (s, 1H), 10.91 (s, 1H), 8.75 (s, 1H), 8.05 (d, *J* = 2.5 Hz, 1H), 7.88 (d, *J* = 9.0 Hz, 1H), 7.70 (dd, *J* = 9.0, 2.4 Hz, 1H), 7.67 – 7.54 (m, 2H), 7.57 – 7.39 (m, 2H), 7.40 – 7.17 (m, 2H), 7.17 – 7.01 (m, 2H), 5.14 (s, 2H). ^{13}C NMR (101 MHz, DMSO-d_6) δ 163.0, 159.7 (d, *J* = 175.5 Hz), 157.8, 156.6, 148.1, 133.2 (d, *J* = 3.0 Hz), 131.6, 130.0 (d, *J* = 8.3 Hz, 2C), 129.8, 126.5, 126.2 (2C, s), 121.2 115.3 (d, *J* = 21.4 Hz, 2C), 114.93, 114.86 (2C, s), 107.1, 68.7. HRMS m/z $[M+H]^+$ calcd for $C_{21}H_{17}N_3O_2F$: 362.1305 found = 362.1290; LC t_R = 4.31 min, >98% Purity.

4-({4-[(3-fluorophenyl)methoxy]phenyl}amino)quinazolin-6-ol (**9**) as a dark green solid (58 %, 174 mg, 0.482 mmol) 138-140 °C; ^{1}H NMR (400 MHz, DMSO-d_6) δ 11.25 (s, 1H), 10.94 (s, 1H), 8.74 (s, 1H), 8.06 (d, *J* = 2.5 Hz, 1H), 7.89 (d, *J* = 9.0 Hz, 1H), 7.71 (dd, *J* = 9.0, 2.4 Hz, 1H), 7.67 – 7.49 (m, 2H), 7.45 (td, *J* = 8.0, 6.0 Hz, 1H), 7.41 – 7.22 (m, 2H), 7.21 – 6.93 (m, 3H), 5.19 (s, 2H). ^{13}C NMR (101 MHz, DMSO-d_6) δ 162.20 (d, *J* = 243.7 Hz), 158.83, 157.80, 156.43, 148.07, 139.93 (d, *J* = 7.4 Hz), 131.62, 130.52 (d, *J* = 8.4 Hz), 129.89, 126.48, 126.26 (2C, s), 123.54 (d, *J* = 2.8 Hz), 121.14, 114.93, 114.87 (2C, s) , 114.63 (d, *J* = 20.9 Hz), 114.23 (d, *J* = 21.9 Hz), 107.13, 68.57 (d, *J* = 1.9 Hz). HRMS m/z $[M+H]^+$ calcd for $C_{21}H_{17}N_3O_2F$: 362.1305 found = 362.1296; LC t_R = 4.25 min, >98% Purity.

4-({4-[(2-fluorophenyl)methoxy]phenyl}amino)quinazolin-6-ol (**10**) as a dark green solid (69 %, 207 mg, 0.573 mmol) 235-237 °C; ^{1}H NMR (400 MHz, DMSO-d_6) δ 11.23 (s, 1H), 10.91 (s, 1H), 8.75 (s, 1H), 8.05 (d, *J* = 2.5 Hz, 1H), 7.88 (d, *J* = 9.0 Hz, 1H), 7.70 (dd, *J* = 9.0, 2.4 Hz, 1H), 7.66 – 7.48 (m, 3H), 7.48 – 7.38 (m, 1H), 7.38 – 7.19 (m, 2H), 7.19 – 7.05 (m, 2H), 5.19 (s, 2H). ^{13}C NMR (101 MHz, DMSO-d_6) 160.4 (d, *J* = 246.1 Hz), 158.8, 157.8, 156.5, 148.1, 131.7, 130.7 (d, *J* = 4.1 Hz), 130.5 (d, *J* = 8.3 Hz), 129.9, 126.5, 126.3 (2C, s), 124.6 (d, *J* = 3.5 Hz), 123.7 (d, *J* = 14.5 Hz), 121.2, 115.4 (d, *J* = 21.0 Hz), 114.9, 114.8 (2C, s), 107.1, 63.8 (d, *J* = 3.7 Hz). HRMS m/z $[M+H]^+$ calcd for $C_{21}H_{17}N_3O_2F$: 362.1305 found = 362.1291; LC t_R = 4.30 min, >98% Purity.

4-((4-((4-fluorobenzyl)oxy)phenyl)amino)quinazolin-7-ol (**11**) as a grey solid (58 %, 174 mg, 0.482 mmol) Decomposed >300 °C; ^{1}H NMR (400 MHz, DMSO-d_6) δ 11.74 (s, 1H), 11.38 (s, 1H), 8.81 – 8.66 (m, 2H), 7.66 – 7.38 (m, 4H), 7.29 (dd, *J* = 6.9, 2.4 Hz, 2H), 7.27 – 7.15 (m, 2H), 7.14 – 7.05 (m, 2H), 5.13 (s, 2H). ^{13}C NMR (101 MHz, DMSO-d_6) δ 164.2, 161.8 (d, *J* = 243.7 Hz), 158.9, 156.5, 150.5, 140.5, 133.2 (d, *J* = 3.0 Hz), 130.0 (d, *J* = 8.3 Hz, 2C), 129.7, 127.1, 126.3 (2C, s), 119.4, 115.3 (d, *J* = 21.4 Hz, 2C), 114.8 (2C, s), 105.8, 102.1, 68.7. HRMS m/z $[M+H]^+$ calcd for $C_{21}H_{17}N_3O_2F$: 362.1305 found = 362.1291; LC t_R = 4.44 min, >98% Purity.

4-((4-((4-fluorobenzyl)oxy)phenyl)amino)quinazoline-6,7-diol (**12**) as a colourless solid (55 %, 158 mg, 0.420 mmol) 285-290 °C; ^{1}H NMR (400 MHz, DMSO-d_6) δ 10.34 (s, 1H), 8.55 (s, 1H), 7.88 (s, 1H), 7.70 – 7.35 (m, 4H), 7.33 – 7.12 (m, 3H), 7.12 – 7.01 (m, 2H), 5.12 (s, 2H). ^{13}C NMR (126 MHz, DMSO-d_6) δ 161.8 (d, *J* = 243.5 Hz), 157.4, 155.7, 154.4, 149.0, 147.7, 137.4, 133.3 (d, *J* = 8.3 Hz, 2C), 130.9, 130.0 (d, *J* = 8.4 Hz, 2C), 125.4, 115.3 (d, *J* = 21.3 Hz, 2C), 114.8 (s, 2C), 107.2, 106.8, 104.6, 68.7. HRMS m/z $[M+H]^+$ calcd for $C_{21}H_{17}N_3O_3F$: 378.1254 found = 378.1240; LC t_R = 4.29 min, >98% Purity.

15. Toxicity cell assay: WS-1 cells were seeded at 400 cells/well in 384 well plates. Cells were treated with compound at 24 h after plating, and cell viability was assessed at 48 h using alamarBlue (ThermoFisher, USA). Fluorescence was measured using Tecan Infinite 200 PRO plate reader with excitation at 535 nM and emission at 590 nM. IC_{50} values were determined by nonlinear regression using Graphpad PrismTM software.
16. Compounds **13-28** prepared as previously described.[11]
17. Compounds **29-34** prepared as previously described.[18]
18. Asquith, C. R. M.; Maffuid, K. A.; Laitinen, T.; Torrice, C. D.; Tizzard, G. J.; Koshlap, K. M.; Crona, D. J.; Zuercher, W. J. *bioRxiv* **2019**, doi: https://doi.org/10.1101/545525